Microkinetic Study of Oxygenate and Hydrocarbon Formation from Syngas on Rhodium and Cobalt Surfaces: Effect of Site Structure on Catalytic Cycles

Neeti Kapur*, Chaitanya Sampara[*], Xianghong Hao*, Jangsuk Hyun*, Bin Shan*, John B. Nicholas[*], Burtron Davis[**] and Kyeongjae Cho[***]

[*]Nanostellar Inc., 3696 Haven Avenue, Redwood City, CA, USA, nkapur@nanostellar.com, xhao@nanostellar.com

[**]Center for Applied Energy Research, University of Kentucky, Lexington, KY, USA, davis@xchange.caer.uky.edu

[***]Department of Materials Science and Engineering, University of Texas at Dallas, Richardson, TX, USA, kjcho@utdallas.edu

ABSTRACT

Rh and Co-based catalysts are known to selectively convert syngas into oxygenates and hydrocarbons under high temperature and pressure conditions. Insights into the mechanistic cycle, structure-reactivity and structure-selectivity correlations required for catalyst design are however, lacking. Herein, we validate reaction networks on Rh and Co surfaces with theoretical and experimental efforts and investigate active site requirements. Microkinetic models are used to investigate competitive routes for forming oxygenates and hydrocarbons on both flat and stepped Rh and Co surfaces. Direct CO dissociation is promoted on defect sites and an alternative hydroxyl methylene based route is kinetically favored for CO activation on flat surfaces for both Rh and Co. Methylene addition to R-CH_2 and CO is deduced to be the precursor for long chain hydrocarbon and C_2-oxygenate formation respectively. Our results indicate that catalytic routes are preferred on step sites irrespective of the reaction considered.

Keywords: steps, methane, ethanol, DFT, kinetics

1 INTRODUCTION

Reforming biomass-derived syngas (mixture of CO and H_2) into fuels and high-value chemicals is an attractive opportunity to diversify away from petroleum and address energy-dependency concerns. Rh-based catalysts used within Fischer-Tropsch (FT) process convert syngas selectively into ethanol and higher oxygenates but suffer from low activity issues [1,2]. On the other hand, hydrocarbons are the predominant products of CO hydrogenation on Co-based materials with moderate turnover rates[1]. Particle size studies report an increase in CO conversion for large Rh and Co particles (~ 6 nm) accompanied by variations in methanol, ethanol, and methane formation rates[3,4]. This enhancement in CO turnover frequency has been attributed to an increase in surface step density under FT operating conditions. However, structure sensitivity of C_1 and C_2 products has not been examined on Rh and Co surfaces. Also, a comprehensive understanding of the underlying catalytic mechanism and active site requirements is essential for developing materials with enhanced activity and product selectivity. However, the elementary reactions involved in dominant routes for CO activation and propagation to methanol, ethanol, methane and ethane on Rh and Co surfaces remain unknown. Herein, we investigate and validate CO hydrogenation network on Rh and Co surfaces with experimental and theoretical efforts and examine the effect of site structure on product formation.

2 METHODOLOGY

Density functional theory (DFT) as implemented in VASP [5] was employed to examine adsorbed structures on Rh(111), Rh(211), Co(0001) and stepped Co surfaces. Three-layered slab surfaces were used to model (2x2) unit cell of Rh(111) and Co(0001) with fixed metal atoms in the lowest layer. Rh(211) was modeled with a eight-layer slab for a (2x1) unit cell. Stepped Co surface was modeled as a three-layered slab for p(4x3) unit cell of Co(0001) with one row missing in the top layer. PAW pseudopotentials and PW91 functional were employed to describe electron-ion interactions and exchange-correlation energies respectively. Transition state calculations were carried out with dimer method and imaginary frequencies were used to confirm these states.

Silica supported Rh and Co (4% metal loading) catalysts used for kinetic studies were supplied by Heraeus and also synthesized onsite using incipient wetness impregnation. These catalysts were reduced under hydrogen before evaluation in fixed bed microreactor (1 g loading) and in slurry based continuously stirred tank reactor (10-40 g loading). CO hydrogenation, C_1-C_4 oxygenate and C_1-C_7 hydrocarbon formation rates were measured on these catalysts at 230-310^{o}C under both atmospheric and high pressure (19 atm) conditions. Products exiting from reactor were detected with FTIR spectrometer. Higher hydrocarbons and oxygenates were analyzed with gas chromatograph-mass spectrometer.

A one dimensional reactor code was used for modeling the steady-state reaction kinetics i.e. exit concentrations for given input. Species balance equation in the axial direction (z) was solved in this model at given temperature as described in equation 1 and 2.

	Rh(111)		Rh(211)		Co(0001)		Stepped Co	
	E_a(eV)	H(eV)	E_a(eV)	H(eV)	E_a(eV)	H(eV)	E_a(eV)	H(eV)
CO(g) → C* + O*	1.07	-0.37	-0.16	-1.16	0.54	-1.2	-0.54	-2.16
CHO* → CH* + O*	1.15	0.07	1.91	-0.08	0.61	-0.89		-0.96
CHOH* → CH* + OH*	0.55	-0.36	0.83	-0.84	0.61	-0.89	0.69	-1.50
CO* + H* →CHO*	1.01	0.81	1.13	0.76	1.31	1.25	0.99	0.87
CHO* + H* → CHOH*	0.57	0.27	0.94	0.51	1.06	0.36	1.32	0.64
CHO* + H* → CH_2O*	0.28	0.13	0.38	0.21	0.38	0.21		0.23
CH_2O* + H* → CH_3O*	0.59	0.15	0.54	0.07	0.90	-0.26		-0.23
CH_3O* + H* → CH_3OH*	0.48	-0.30	0.96	0.18	1.36	0.66		1.02

Table 1. Kinetic barriers (E_a) and reaction enthalpies (H) for CO activation and methanol formation routes on flat and stepped Rh and Co surface.

$$\frac{w}{A}\frac{dx_{g,i}}{dz} = -k_{m,i}S(x_{g,i} - x_{s,i}) = \sum_{j=1}^{reactions} a_j s_{ij} r_j \qquad (1)$$

$$\frac{d\theta_i}{dt} = \sum_{j=1}^{reactions} s_{ij} r_j \qquad (2)$$

where w and A are the molar flow rates and reactor face area respectively. Mole fraction of species *i* in gas phase and on catalyst surface are represented by $x_{g,i}$ and $x_{s,i}$ respectively. Other inputs for this equation include mass transfer coefficient ($k_{m,i}$), surface area per reactor volume (S), active site density for reaction *j* (a_j), stoichiometric coefficient for species *i* in reaction *j* (s_{ij}) and reaction rate (r_j). Boundary condition is defined at reactor inlet by specifying mole fraction of different species in the feedstream. Reaction rates (r_j) required for the model were written based on the hypothesized mechanism in terms of rate constants and surface coverage (θ_i). DFT-based activation barriers and pre-exponential factors were used as the first-order approximation for the rate constants. The steady state solution from this microkinetic solver provides the exit concentrations. These concentrations were used within the optimization loop, which minimizes the difference between calculated and experimental exit concentrations for all tested conditions by modifying the rate constants [6,7].

3 RESULTS & DISCUSSION

In this study, DFT calculations were employed to investigate reaction mechanisms for CO activation, oxygenate (methanol, ethanol) and hydrocarbon (methane, ethane) formation on Rh and Co surfaces. Favorable sites for C-O bond breaking and C-H, C-C bond making reactions were deduced by comparing reaction kinetics and energetics on flat and stepped surfaces. Next, we compared DFT-derived lowest energy pathways against experimental kinetic data within microkinetic models. Experimental and simulated turnover rate trends were compared for mechanism verification and deducing rate limiting reactions.

3.1 CO activation on Rh & Co surfaces

Binding energies for C_1 and C_2 intermediates ($C_xH_yO_z$) on Co and Rh surfaces are determined to be stronger on step sites due to their low coordination as compared to the flat surfaces. CO adsorbs on an atop site on Rh(111) with a binding energy of 1.75 eV and on step edge-atop site on Rh(211) with a binding energy of 2.03 eV [8]. CO dissociation proceeds without barrier with respect to CO(g) on Rh(211) surface resulting in atomic carbon and oxygen formation. This mechanism however, requires 1.1 eV of energy to overcome the kinetic barrier on Rh(111) (Table 1). Hence, alternative H-assisted CO dissociation mechanisms were examined on Rh terraces.

Hydrogen molecule dissociates spontaneously into hydrogen atoms on Rh and Co surfaces, which are readily available for addition reactions. CO can hydrogenate to formyl (CHO) and hydroxyl methylidyne (COH) intermediates but the associated C-O scission barriers are still higher than 1 eV (CHO* → CH* + O*). Instead CHO can hydrogenate to hydroxyl methylene (CHOH) on Rh(111) which leads to an increase in the C-O bond length to 1.37 Å as compared to 1.16 Å in adsorbed CO. The associated C-O activation barrier in CHOH also decreases to 0.55 eV. Hence, CO* → CHO* → CHOH* → CH* + OH* is the favorable pathway for CO activation on Rh(111) surface. Overall, Rh step sites are kinetically more favorable for CO dissociation. Therefore, for larger Rh nanoparticles with more step sites, CO turnover frequency will increase.

On Co(0001) surfaces, CO adsorbs on three-fold hollow sites with a binding energy of 1.8 eV while on stepped Co surface, CO binds on step edge-atop site with binding energy of 1.87 eV. Similar to Rh, carbene mechanism (CO → C* + O*) is determined to be favorable on stepped Co surface while hydroxyl methylene based mechanism is found to be responsible for C-O scission on Co(0001). CO dissociation is also more exothermic on Co as compared to Rh stepped surfaces due to stronger atomic carbon binding and therefore, Co is thermodynamically more driven towards CO activation.

3.2 Structure sensitivity of C_1 and C_2 products on Rh & Co surfaces

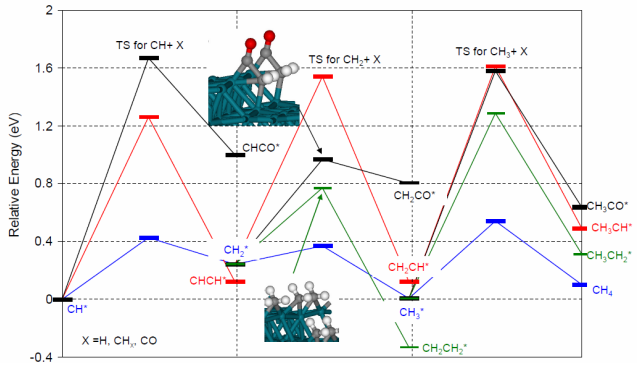

Figure 1. Reaction energetics for hydrogenation, CH_x addition and CO insertion on Rh(211) surface.

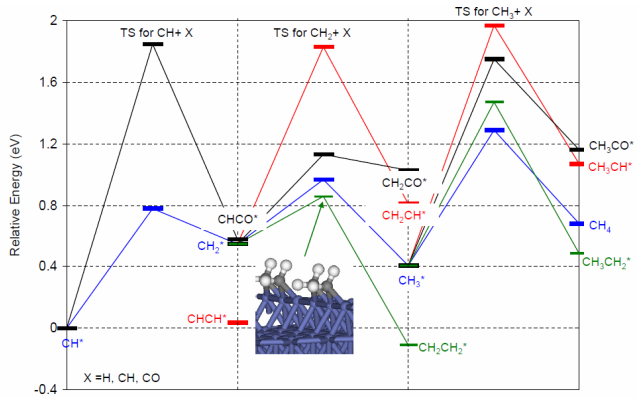

Figure 2. Reaction energetics for hydrogenation, CH_x addition and CO insertion on stepped Co surface.

Product formation trends on Rh and Co step sites are deduced from Figure 1 and 2. Atomic carbon resulting from CO dissociation hydrogenates to methylidyne (CH) with a barrier of 0.56 eV and 0.76 eV on stepped Rh and Co surfaces respectively. CH hydrogenation to methylene (CH_2), methyl (CH_3) and finally methane (CH_4) on both Co and Rh involves barriers lower than those required for C-C bond formation. Transition state for CH_3 + H corresponds to the highest energy state for methane formation and is therefore, the rate determining step. CH_x addition to CH, CH_2 and CH_3 intermediates was examined extensively. The lowest barrier for C-C coupling corresponds to CH_2 + CH_2 reaction on both Co and Rh step sites resulting in exothermic ethylene (CH_2CH_2) formation. Ethylene can desorb, hydrogenate to ethane or act as a monomeric chain for longer hydrocarbons. CO insertion into CH_2 results in endothermic formation of CH_2CO and has lower barriers than CH + CO and CH_3 + CO. These C-H and C-C bond formation barriers on Rh and Co step sites result in lower energy states as compared to Rh and Co terraces (results not shown here) due to stronger binding energies. Based on the relative energetics for hydrogenation, CH_x addition and CO insertion reactions in Figures 1 and 2, methane is determined to be the dominant product followed by hydrocarbons and oxygenates on Rh and Co. This product formation trend is in agreement with the experimental rates reported by Quyoum et al [2]. Also, low coordinated Rh and Co step edge sites are actively engaged in the transition states for C-H and C-C bond formation reactions shown in insets for Figures 1 and 2.

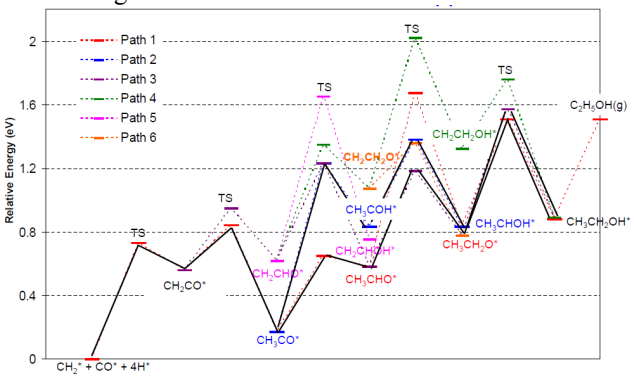

Figure 3. Reaction pathways for ethanol formation on Rh(211) surface.

Since ethanol (CH_3CH_2OH) is selectively formed on Rh sites, we have investigated multiple hydrogenation pathways beyond CH_2CO formation as detailed in Figure 3. CH_2CO intermediate preferentially hydrogenates to acyl (CH_3CO). Further hydrogenation can lead to either CH_3CHO or CH_3COH intermediates. Since CH_3CHO has a low decomposition barrier to CH_3CO, CH_3COH based pathway to CH_3CH_2OH has a higher probability. Similar analysis for ethanol formation on Rh terraces leads to the following hydrogenation pathway: CH_2CO → CH_2CHO → CH_2CH_2O → CH_3CH_2O → CH_3CH_2OH. Hence, ethanol formation is determined to be structure sensitive on Rh sites. We have also determined methanol formation to be structure sensitive on Rh and Co sites (Table 1). Lowest energy pathway for methanol is determined to be identical on Rh terrace and (211) sites: CO → CHO → CH_2O → CH_3O → CH_3OH but the hydrogenation barriers are dependent on the site structure (not shown here). Similar trend is found for methanol formation on Co flat and stepped surfaces in agreement with previous literature [5].

By combining these reaction routes leading to methane, ethanol and hydrocarbons, we can map out the reaction network from CO to products on Rh and Co sites for microkinetic modeling.

3.3 Microkinetic model example: CH_4/Rh

Herein, we report results for the validation of methane formation mechanism on Rh surfaces with microkinetic modeling. Table 2 includes the reaction network and associated forward and reverse barriers leading to CH_4 formation. These values were used as the input for microkinetic solver (Equations 1, 2).

	$E_{forward}$(eV)	$E_{reverse}$(eV)
$CO(g) + * \rightarrow CO*$	0	1.0
$H_2(g) + 2* \rightarrow 2H*$	0	1.2
$CO* + * \rightarrow C* + O*$	0.87	1.0
$C* + H* \rightarrow CH* + *$	0.56	0.75
$CH* + H* \rightarrow CH_2* + *$	0.43	0.19
$CH_2* + H* \rightarrow CH_3* + *$	0.13	0.36
$CH_3* + H* \rightarrow CH_4 + 2*$	0.53	-
$O* + H* \rightarrow OH* + *$	0.52	0.77
$OH* + H* \rightarrow H_2O* + *$	0.86	0.59
$H_2O* \rightarrow H_2O(g) + *$	0.70	-

Table 2. Forward ($E_{forward}$) and reverse ($E_{reverse}$) barriers for hypothesized methane formation mechanism on Rh surface.

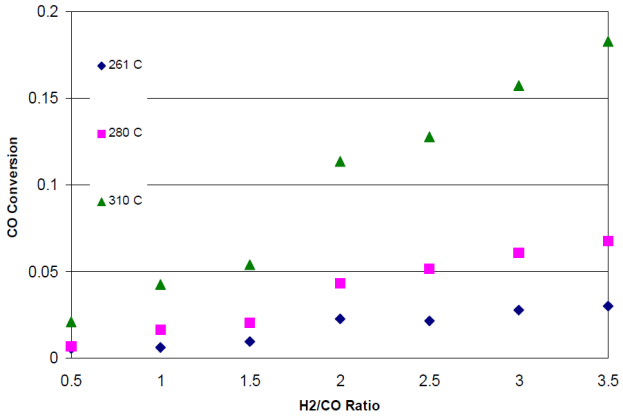

Figure 4. CO conversion as a function of temperature and H_2/CO ratio measured under atmospheric pressure in a fixed bed reactor.

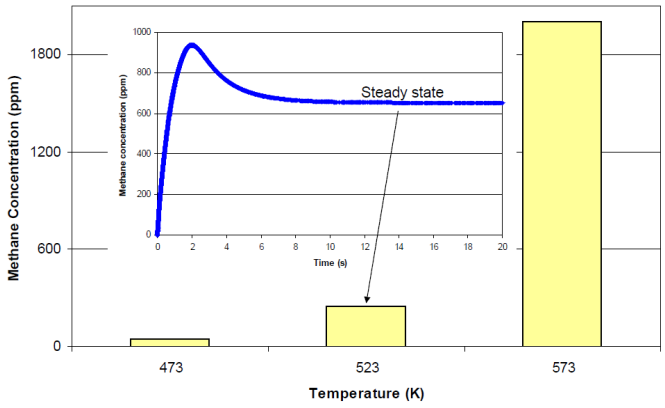

Figure 5. Steady state methane concentration determined as a function of temperature and H_2/CO =1 for microkinetic model detailed in Table 2. Inset shows the methane concentration profile as a function of time at 523 K and H_2/CO =1.

Figure 5 reports the steady state methane concentrations for an inlet feed with 3% CO and H_2/CO =1 at different temperatures. These results show an increase in CH_4 concentrations at reactor outlet with increase in temperature since CO activation and hydrogenation rates are enhanced. Also, based on the mechanism in Table 2, increase in H* surface concentration will increase product formation rate.

We also report the experimental CO conversion observed at different temperatures and H_2/CO ratios in Figure 4. The dominant product of CO hydrogenation on Rh under 1 atm and 261-310^{o}C is methane and the product distribution shows small amounts of C_2-C_4 hydrocarbons (not shown). These experimental trends show an increase in conversion with temperature and amount of H_2 in feed. We can therefore, conclude that the simulated model trends are concurrent with the experimental observations. However, optimization procedure has to be performed to tune microkinetic parameters for quantitative agreement between these results.

4 CONCLUSIONS

Direct CO dissociation is promoted on defect sites and an alternative hydroxyl methylene based route is established to be kinetically favored on Rh and Co flat surfaces. Methylene addition to R-CH_2 and CO is deduced to be the precursor for hydrocarbon growth and C_2 oxygenate formation respectively on Rh and Co step sites. Different intermediates are involved in hydrogenation of ketene (CH_2CO) to ethanol on flat and stepped Rh surfaces, thus demonstrating structure sensitivity. In summary, step sites provide a lower route for CO activation, methane, methanol, ethanol and hydrocarbon formation and are preferred irrespective of the bond breaking/making (C-H, C-C, C-O) reaction considered. The reaction routes and associated barriers deduced on Rh and Co sites can be used as an input for microkinetic modeling. Kinetics for methane formation mechanism on Rh sites is verified by comparing solutions from microkinetic solver for temperature and H_2/CO ratio variations with experimental trends.

REFERENCES

1. R. Burch, M. Petch, Appl. Catal. A (1992) 88, 39.
2. R. Quyoum, V. Berdini, M. Turner, H. Long, and P. Maitlis, J. Catal. (1998) 173, 355.
3. H. Arakawa, K. Takeuchi, T. Matsuzaki, and Y. Sugi, Chem. Lett. 9 (1984) 1607; S. Zhou, H. Zhao, D. Ma, S. Miao, M. Cheng, and X. Bao, Z. Phys. Chem. 219 (2005) 949.
4. J. den Breejen, P. Radstake, G. Bezemer, J. Bitter, V. Frøseth, A. Holmen and K. de Jong, JACS (2009) 131, 7197.
5. G. Kresse, J. Furthmüller, Phys. Rev. B (1996) 54, 11169.
6. C. Sampara, E. Bisset, M. Chmielewski, D. Assanis, Ind. Eng. Chem. Res. (2007) 46, 7993.
7. C. Sampara, E. Bisset, D. Assanis, Chem. Eng. Sci. (2008) 63, 5179.
8. N. Kapur, J. Hyun, B. Shan, J. B. Nicholas and K. Cho, J. Phys. Chem. C, submitted.